Periodic Textures of Nematic Polymers and Orientational Slip

Alejandro D. Rey

Department of Chemical Engineering, McGill University, Montreal, Quebec, Canada H3A 2A7

Received January 2, 1991; Revised Manuscript Received April 1, 1991

ABSTRACT: Nonlinear numerical analysis predicts that when a uniformly oriented nematic polymer, placed between parallel isotropic untreated surfaces, is subjected to a sufficiently strong magnetic field normal to the initial polymer orientation, a transient periodic pattern develops. The transient nematic polymer orientation at the surface is found from the Euler-Lagrange equation for surface motion. The dynamics of the polymer at the surface is characterized by the ratio of the surface-polymer characteristic time to the bulk characteristic time, B. The actual response is limited by that of an orientational free surface ($B = 0$) and that of fixed polymer surface orientation ($B \Rightarrow \infty$). The magnitude of B has no effect on the field dependence of the observed wavelength. In the high-field regime, the dynamics of the velocity and bulk orientation and the final polymer orientation are independent of B. In the low-field regime, the dynamics of the velocity and bulk orientation, the strength of the flows, and the final polymer orientation are strongly dependent on B.

1. Introduction

Nematic polymers are characterized by the high anisotropy of their viscoelastic properties. A consequence of this anisotropy is the presence of transient periodic textures during the decay from an unstable state.[1-3] For example, when a nematic polymer is subjected to a magnetic field normal to the initial average molecular orientation, described by the director **n**, the fastest decrease of the magnetic energy results in transient banded textures when viewed with a microscope between crossed polarizers.

In this paper, we analyze the planar periodic twist magnetic instability that is observed[4] when a nematic polymer, placed between two thinly spaced parallel, untreated, glass plates and with the director parallel to the surfaces and aligned in one direction, is subjected to a sufficiently strong magnetic field normal to the initial orientation; when the sample is observed between cross polars, a periodic pattern consisting of dark bands separated by light bright bands develops, and the separation between the dark bands is the half-wavelength of the periodic pattern. We restrict our attention to rigid, rodlike, nematic liquid-crystalline polymers of positive anisotropic magnetic susceptibility and to the case in which the director orients in the direction of the field but remains at all times parallel to the bounding surfaces; other nonplanar complex textures that have been reported[5,6] are beyond the scope of this paper. The wavelength of the transient periodic pattern that develops depends on the cell spacing, the magnetic field strength, the viscoelastic properties of the nematic polymer, and the surface condition. The linear analysis of the planar periodic twist magnetic instability for fixed director orientation at the surfaces was given by Lonberg and Meyer[7] and the corresponding nonlinear numerical analysis by Rey and Denn.[8] It has been shown[7] that the transient periodic response is due to strong coupling between director reorientation and fluid flow, in which opposed rotating domains produce shear flows characterized by lower viscosities than that involved in pure rotation. The viscous mechanism favors short wavelengths, while the elastic response favors longer wavelengths. The competing effects find an optimal balance, at which the total free energy decreases fastest. The instability has been studied experimentally for a series of nematic polymers in cells without[4-6] and with surface treatment.[2,9] A quantitative comparison between numerical nonlinear analysis and experiments, using poly(benzyl glutamate) (PBG) as a model compound, and a surface treatment that produces parallel fixed surface director orientation is given by Srajer et al.[9] They show that for a given field intensity the experimentally observed wavelength is longer than that predicted by the linear theory but is in excellent agreement with that predicted by the nonlinear numerical analysis; the discrepancy is large at high fields but decreases with decreasing field strengths. Fincher[4] performed an experimental study of the planar periodic twist instability using poly(1,4-benzamide) (PBA) and thinly spaced (25-1000-μm) untreated glass surfaces. He shows that there is a large discrepancy at high field strengths from the magnetic field-wavelength scaling predicted by the linear theory[7] but good agreement at low fields. Since it is not known a priori if the reported discrepancy[4] is due to the neglected nonlinearities or to existing surface-polymer interactions, it is necessary to perform a nonlinear numerical analysis using time-dependent director boundary conditions, appropriate for the case of untreated isotropic surfaces. Furthermore, if the instability is to be used to measure, with any degree of accuracy, some of the viscoelastic properties of nematic polymers, we should know the effects of the polymer-surface interaction on the dynamics of the director and velocity field when using untreated surfaces.

The static interaction between a nematic liquid crystal and the bounding surfaces can be described macroscopically by a surface free energy composed of a surface deformation energy due to director gradients and a coupling energy of the director at the interface.[10] The surface deformation energy arises due to director surface gradients and is introduced by surface elastic constants. The coupling energy is the part of the surface energy that depends on the director orientation with respect to the easy axis of the surface; the direction of the easy axis depends on the specific liquid crystal-surface system and on the surface treatment.[10] When the director is aligned with the easy axis, the coupling energy is a minimum; the anchoring strength W is the coefficient introducing the coupling energy.[11] When $W \Rightarrow \infty$, the director aligns along the easy axis (strong anchoring), while for finite W the time-dependent director orientation is the solution to the balance of surface elastic and viscous torques. The elastic torques at the surface appear due to bulk distortions impressed onto the surface, deviations from the easy axis of the surface, and director surface gradients. Viscous

0024-9297/91/2224-4450$02.50/0

Table I
Physical Constants for PBG[9]

Viscosities, P	
α_1[a]	−47.24
α_2	−69.2
α_3	0.18
α_4	3.48
α_5	66.1
α_6	−2.92
$\gamma_1 = \alpha_3 - \alpha_2$	69.3
$\gamma_2 = \alpha_6 - \alpha_5$	−69.03
Elastic Constants, 10^{-7} dyn	
K_{11}	12.1
K_{22}	0.78
K_{33}	7.63

[a] Estimated by using the Marruci hard rod theory[21] with an order parameter $S = 0.8$.

surface torques appear due to the transient director reorientation at the surface and are introduced by surface viscosities. Dissipative interactions between a rotating director and the surface have already been formulated.[12,13]

For entropic reasons, the planar alignment of the director at a surface has been shown to be the most likely for high molecular weight nematics.[14] This appears to be the case for PBA[4,15,16] and for poly(1,4-phenylene-2,6-benzobis(thiazole)) (PBT)[5], although it is not for poly(benzyl L-glutamate) (PBLG).[17] Since we are restricting the analysis to the planar periodic twist instability with untreated isotropic surfaces, we shall assume that any direction contained by the surface is an easy axis.[4] Therefore, no contribution from the surface coupling energy is considered. We neglect surface deformation energy contributions since there are no experimental reports, to the author knowledge, of its existence for nematic polymers. With these two assumptions, the transient director surface orientation is given by a balance of elastic torques from bulk deformations and viscous surface torques about an axis normal to the surface. At the surface, the director is undergoing rotations (orientational slip) but without positional displacements (no positional slip). The time scale of surface reorientation depends partly on the magnitude of the surface viscosities; the two limiting cases correspond to zero surface viscosity (orientational free surface) and infinite surface viscosity (fixed surface orientation). The questions to be answered in this work are how does the wavelength selection, the dynamics of the director and velocity fields, and the final state of the system change as we let the surface viscosity sample the range limited by the two cases mentioned above.

The purpose of these paper is (i) to derive the time-dependent boundary conditions for the director of a rigid-rod nematic polymer undergoing the planar periodic twist instability with untreated isotropic bounding surfaces, (ii) to present the predictions of a numerical nonlinear analysis using (i), and (iii) to provide an explanation for the discrepancy reported by Fincher.[4]

2. Balance Equations and Boundary Conditions

The periodic twist instability is best described in Cartesian coordinates (x',y',z'); see Figure 1. The computational cell consist of two parallel bounding surfaces separated by a distance D along the y' direction and two vertical nematic surfaces separated by a distance L, the half-wavelength of the periodic pattern, along the z' direction. The initial director field is $\mathbf{n}(y',z',t'=0) = (0,0,1)$, and at time $t' = 0$, a field of sufficient strength is applied normal to the initial director orientation, $\mathbf{H} = (H,0,0)$. The kinematics of the periodic response is described by the director field $\mathbf{n}(y',z',t') = (\sin\theta,0,\cos\theta)$, and the re-

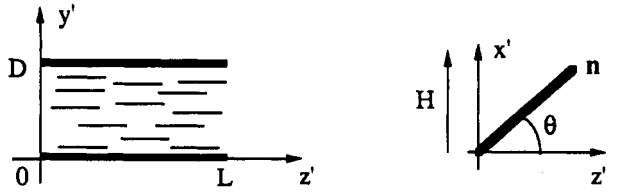

Figure 1. Schematic diagram of the nematic polymer cell at $t' = 0$ and definition of the coordinates. The applied field is in the x' direction. Cell surfaces are at $y' = 0$ and D.

orientation driven flow field $\mathbf{v}(y',z',t') = (u',0,0)$. Since the detailed derivation has been given,[2] here we present the final expressions for the balance equations. The dimensionless angular and linear momentum balance equations are

$$\frac{h'}{2}\left(\frac{\partial\theta}{\partial z}\right)^2 + h\frac{\partial^2\theta}{\partial z^2} + \hat{K}_{22}A^2\frac{\partial^2\theta}{\partial^2 y} - \frac{\partial\theta}{\partial t} - \frac{1}{2}(\lambda\cos\theta - 1)\frac{\partial u}{\partial z} + \frac{1}{2}\sin 2\theta = 0 \quad (1)$$

$$\eta_1\frac{\partial^2\theta}{\partial z\partial t} + \eta_2\frac{\partial\theta}{\partial z}\frac{\partial\theta}{\partial t} + \eta_3A^2\frac{\partial\theta}{\partial y}\frac{\partial u}{\partial y} + \eta_4\frac{\partial\theta}{\partial z} + \eta_5\frac{\partial^2 u}{\partial z^2} + \eta_6A^2\frac{\partial^2 u}{\partial y^2} = 0 \quad (2)$$

Here

$$h = [K_{11}\sin^2\theta + K_{33}\cos^2\theta]/(\chi_aH^2L^2); \quad h' = [K_{11} - K_{33}]\sin 2\theta/(\chi_aH^2L^2) \quad (3)$$

$$\hat{K}_{22} = K_{22}/(\chi_aH^2L^2); \quad u = u'\gamma_1/(\chi_aH^2L); \quad t = t'(\chi_aH^2)/\gamma_1; \quad z = z'/L; \quad y = y'/D; \quad A = L/D \quad (4)$$

$$\eta_i = \eta_i'/\gamma_1, \quad i = 1, ..., 6; \quad \lambda = \gamma_2/\gamma_1 \quad (5)$$

where the $\{\eta_i\}$, $i = 1, ..., 6$, tabulated in the Appendix, are functions of the director orientation and the six Leslie torque coefficients, γ_1 and γ_2 are the rotational and irrotational torque coefficients, χ_a is anisotropic magnetic susceptibility, and the $\{K_{ii}\}$, $i = 1$–3, are the Frank elastic coefficients for splay, twist, and bend, respectively.[11]

In analogy with bulk motion,[18] assuming the no positional slip condition ($v = 0$) at the surface, the Euler–Lagrange equation of surface motion of the director is, for the present case,

$$\frac{\partial R^s}{\partial\dot{\theta}} + \Phi_\theta = 0 \quad (6)$$

where R^s is the surface Rayleigh dissipation function, θ (director orientation) is the only generalized coordinate, and Φ_θ is the generalized elastic force; a superposed dot denotes time differentiation. $\partial R^s/\partial\dot{\theta}$ is the frictional force and is a linear function of the velocities.[18] Therefore, R^s is chosen as

$$R^s = \frac{\lambda^s}{2}(\dot{n}_x^2 + \dot{n}_z^2) = \frac{\lambda^s}{2}\dot{\theta}^2 \quad (7)$$

where λ^s is the surface viscosity for surface planar director reorientations. The frictional force acting on the director due to orientational slip is

$$\partial R^s/\partial\dot{\theta} = \lambda^s\dot{\theta} \quad (8)$$

The elastic force Φ_θ is obtained from the surface contribution to the variation of the total elastic free energy of the system.[19] For the present geometry, the total free

energy F, neglecting kinetic ($\rho v^2 = 0$) and surface energies contributions, in a volume V' of nematic polymer under the presence of a magnetic field, is[11]

$$F\left(\theta,\frac{\partial\theta}{\partial y'},\frac{\partial\theta}{\partial z'}\right) = \int_{V'}\Lambda\left(\theta,\frac{\partial\theta}{\partial y'},\frac{\partial\theta}{\partial z'}\right)dV' = \int_{V'}\left(\Lambda_e\left(\theta,\frac{\partial\theta}{\partial y'},\frac{\partial\theta}{\partial z'}\right)+\Lambda_m(\theta)\right)dV' \quad (9a)$$

$$\Lambda = \Lambda_e + \Lambda_m \quad (9b)$$

$$\Lambda_e = \frac{1}{2}K_{22}\left(\frac{\partial\theta}{\partial y'}\right)^2 + \frac{1}{2}(K_{11}\sin^2\theta + K_{33}\cos^2\theta)\left(\frac{\partial\theta}{\partial z'}\right)^2 \quad (9c)$$

$$\Lambda_m = -\frac{1}{2}\chi_a H^2\sin^2\theta \quad (9d)$$

where Λ, Λ_e, and Λ_m are the total free-energy density, the elastic free-energy density due to bulk deformations, and the magnetic free-energy density, respectively. In the Appendix, we show that the saddle-splay contribution to elastic free-energy density Λ_e is zero for the present case. The variation of F is

$$\delta F = \int_{V'}\left[\frac{\partial\Lambda}{\partial\theta}\delta\theta + \frac{\partial\Lambda_e}{\partial\theta,_i}\delta\theta,_i\right]dV' \quad (10)$$

where a comma denotes partial differentiation and $i = x'$, y', z'. Using the Gauss theorem, δF becomes

$$\delta F = \int_{V'}\left[\frac{\partial\Lambda}{\partial\theta}\delta\theta - \frac{\partial}{\partial i}\left(\frac{\partial\Lambda_e}{\partial\theta,_i}\right)\delta\theta\right]dV' + \int_{S'}\left[\frac{\partial\Lambda_e}{\partial\theta,_i}\nu_i\delta\theta\right]dS' \quad (11)$$

where ν is the outward unit normal vector to the enclosing surface S' of volume V'. The generalized elastic forces Φ_θ due to bulk deformations, at the two bounding surfaces, are given by

$$\Phi_\theta = \frac{\partial\Lambda_e}{\partial(\partial\theta/\partial i)}\nu_i = \pm\frac{\partial\Lambda_e}{\partial(\partial\theta/\partial y')} = \pm K_{22}\frac{\partial\theta}{\partial y'} \quad (12)$$

where the + (−) refers to the top surface (bottom surface) located at $y' = D$ ($y' = 0$). Finally, the dimensionless Euler–Lagrange equation (eq 6) for the transient director upper ($y = 1$) and lower ($y = 0$) surface orientation becomes

$$B\frac{\partial\theta}{\partial t} = -\frac{\partial\theta}{\partial y} \quad \text{at} \quad y = 1, \quad 0 \le z \le 1 \quad (13a)$$

$$B\frac{\partial\theta}{\partial t} = \frac{\partial\theta}{\partial y} \quad \text{at} \quad y = 0, \quad 0 \le z \le 1 \quad (13b)$$

Here

$$B = \left(\frac{D\lambda^s}{K_{22}}\right)\Big/\left(\frac{\lambda_1}{\chi_a H^2}\right) = \tau^S/\tau^b \quad (14)$$

is the ratio of the bounding surface–polymer interface characteristic time τ^S and the bulk characteristic time τ^b for director reorientation. Since bulk deformations are driving the surface deformations, when $B < 1$ the actual time scale for surface director reorientation is bounded by τ^b. For a finite H, there are three representative cases: (1) $B = 0$ corresponds to an orientational free surface for which $\partial\theta/\partial y = 0$, (2) $B = 1$ shows the case when the two time scales may be equal, (3) $B \Rightarrow \infty$ corresponds to the case of fixed director orientation since $\partial\theta/\partial t = 0$ and the director will retain the initial orientation. Since there are no reports in the literature, to the author's knowledge, on surface viscosities of nematic polymers on glass plates, a parametric study of the three cases seems appropriate. We nevertheless may expect that, for actual rigid rodlike nematic polymers, isotropic glass surfaces, and finite fields, $1 < B \ll \infty$.

Equations 1 and 2 are solved with the following boundary conditions: (13a), (13b), and

$$\partial\theta/\partial z = 0 \quad \text{at} \quad 0 \le y \le 1, \quad z = 0 \quad (15a)$$

$$\partial\theta/\partial z = 0 \quad \text{at} \quad 0 \le y \le 1, \quad z = 1 \quad (15b)$$

$$u = 0 \quad \text{at} \quad y = 0, \quad 0 \le z \le 1 \quad (15c)$$

$$u = 0 \quad \text{at} \quad y = 1, \quad 0 \le z \le 1 \quad (15d)$$

$$u = 0 \quad \text{at} \quad 0 \le y \le 1, \quad z = 0 \quad (15e)$$

$$u = 0 \quad \text{at} \quad 0 \le y \le 1, \quad z = 1 \quad (15f)$$

using Galerkin finite elements with bilinear basis functions over 10 elements in each coordinate. The time integration scheme was a first-order implicit Euler predictor–corrector method.[20] The material constants used are shown in Table I and are those of poly(γ-benzyl glutamate)[9] except α_1, which was estimated by using Marruci's hard rod theory;[21] the magnetic susceptibility $\chi_a = 7.19 \times 10^{-9}$ emu/mol,[9,22] the cell thickness is $D = 0.005$ cm.

3. Numerical Results

Parametric studies were performed for different surfaces (B), field intensities (H), and scaled half-wavelengths ($A = L/D$); for given H and B, we studied the evolution of $\mathbf{n}$ and $\mathbf{v}$ for various values of A. The minimum field intensity for the planar periodic twist instability[2] is $H^* = 1 + K_{33}\alpha_4\gamma_1/2\alpha_2{}^2K_{22}$, which for the present case gives $H^* = 2.068 \times 10^3$ G. In this paper, we present the results for the two representative cases, $H = 1.12H^* = 2.31 \times 10^3$ (low-field long-wavelength regime) and $H = 3.44H^* = 7.12 \times 10^3$ G (high-field short-wavelength regime), and for the three representative surface conditions, $B = 10^{-6}$ (orientational free surface), $B = 1$ (equal surface and bulk characteristic times), and $B = 10^6$ (fixed director orientation). For the chosen computational cell, the amplitudes of the director and dimensionless velocity are given by $\theta(0.5,0)$ and $u(0.5,0.5)$. The response for each H and B is compared with that of the linear mode, which is obtained by solving the nonlinear boundary value problem stated above, with the value of A obtained from the linear theory.[2]

3.1. High-Field Short-Wavelength Regime. The director orientation $\theta(0.5, 0)$ as a function of time is shown in Figure 2, for $A = 1.4$ (linear theory), 2.0, and 2.5 and for the three representative surfaces. The corresponding maximum dimensionless velocity $u(0.5,0.5)$ as a function of time is shown in Figure 3. The parts of the figure show that at high fields there is no effect of the surface condition on the magnitude and dynamics of the director and velocity amplitudes. This insensitivity to the surface condition follows from the scaled equations (1) and (2); at high fields ($A \Rightarrow 0$), the field variations in the y direction are negligible and the bulk response is dominated by gradients in the z direction; in other words, there is a relative weak transmission of torques in the y direction when compared with the transmission in the z direction. The figures show that the linear mode (full line) is fastest at early times, but at later times modes of longer wavelength (dashed line) are faster than the linear mode, in agreement with previous results.[9] It is now known[9] that the selected wavelength optimizes the kinetic (flow) and thermodynamic (elasticity) mechanisms at early times but at later times mainly the thermodynamic one. The figures show that periodic director reorientations of longer wavelengths are slower at early times due to weaker flows but faster at later times due to more director alignment in the direction of the applied field. If the wavelength is too long (dashed-dot line), by the time the corresponding mode becomes the

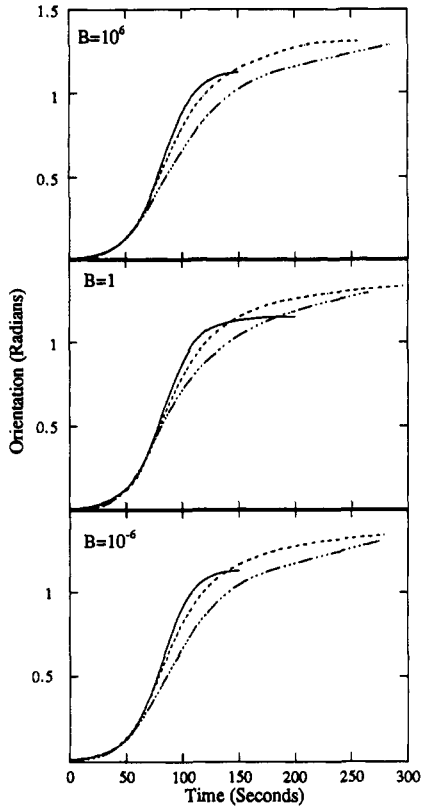

Figure 2. Orientation $\theta(0.5, 0)$ of the director as a function of time, for $B = 10^6$, 1, and 10^{-6}. $H = 7.12 \times 10^3$ G; (—) $A = 1.4$ (linear); (- - -) $A = 2$; (—···—) $A = 2.5$.

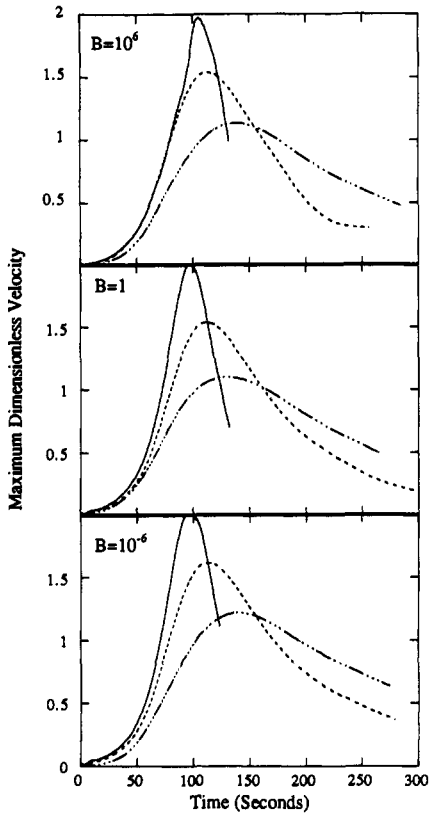

Figure 3. Maximum dimensionless velocity $u(0.5,0.5)$ as a function of time, for $B = 10^6$, 1, and 10^{-6}. $H = 7.12 \times 10^3$ G; (—) $A = 1.4$ (linear); (- - -) $A = 2$; (—···—) $A = 2.5$.

fastest, the pattern is already formed. The pattern that forms consists of an array of splay-bend inversion walls.[8] Therefore, the wavelength switches[9] from the one given by the linear theory at early times to the actually observed longer wavelength that corresponds to the fastest decrease

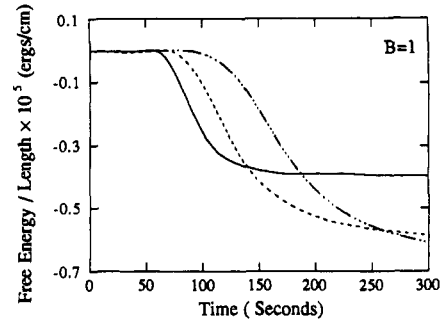

Figure 4. Free energy per unit length in the x direction as a function of time, for $B = 1$. $H = 7.12 \times 10^3$ G; (—) $A = 1.4$ (linear); (- - -) $A = 2$; (—···—) $A = 2.5$. The free energies per unit length in the x direction are normalized with respect to the linear mode ($A = 1.4$): $F_2^* = 1.4F_2/2$, $F_{2.5}^* = 1.4F_{2.5}/2.5$.

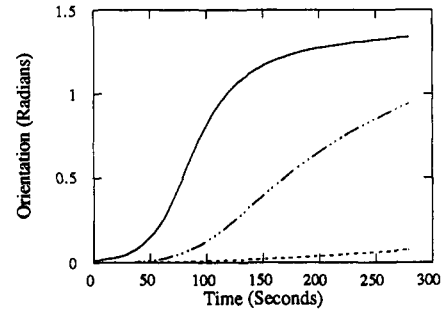

Figure 5. Comparison between representative bulk and surface director dynamics. Orientation of the director as a function of time, for $A = 2$. $H = 7.12 \times 10^3$ G; (—) bulk director orientation $\theta(0.5,0)$, $B = 1$; (- - -) surface director orientation $\theta(1,0)$, $B = 1$; (—···—) surface director orientation $\theta(1,0)$, $B = 10^{-6}$.

in the free energy at the time at which the pattern forms. The total free energy per unit length in the x direction,[11]

$$F/\text{length} = \int_0^1 \int_0^1 \left\{ A\left(\frac{1}{2}K_{22}\left(\frac{\partial\theta}{\partial y}\right)^2\right) + \frac{1}{A}\left(\frac{1}{2}(K_{11}\sin^2\theta + K_{33}\cos^2\theta)\left(\frac{\partial\theta}{\partial z}\right)^2\right)\right\} dy\,dz + \int_0^1 \int_0^1 \left\{\frac{L^2}{A}\left(-\frac{1}{2}\chi_a H^2 \sin^2\theta\right)\right\} dy\,dz \quad (16)$$

for each A is normalized with respect to the linear mode; i.e., $F^*_{A=2}/\text{length} = F_{A=2}/\text{length} \times 1.4/2$, and the results are plotted as a function of time for $B = 1$ in Figure 4. In agreement with Figure 2, the linear mode is faster up to 130 s, at which time the $A = 2$ mode is able to decrease the total free energy at a faster rate; therefore, the wavelength actually observed is longer than that corresponding to the linear mode. Note that the pattern is essentially formed by the time the $A = 2.5$ mode becomes the fastest.

The surface dynamics of the $A = 2$ mode are summarized in Figure 5, where we plot the amplitude of the director field $\theta(0.5,0)$ for $B = 1$ and the director maximum surface orientation $\theta(1,0)$ for $B = 1$ and 10^{-6} as a function of time. Even for the case of $B = 10^{-6}$, the reorientation is much slower at the surface than in the bulk. This again reflects the fact that there is a weak transmission of torques in the y direction from the bulk into the surface due to the relatively small values of A.

The evolution of the director $\theta(y = 0.5,z)$ profiles at the midplane as a function of the dimensionless distance z is shown in Figure 6, for $A = 1.4$ and $B = 1$. The periodic distortions indicate clockwise director rotations for $z < 0.5$, and anticlockwise rotations for $z > 0.5$. Even at long times, there are strong elastic torques being transmitted in the z direction since only at $z = 0$ and $z = 1$ is $\partial\theta/\partial z$

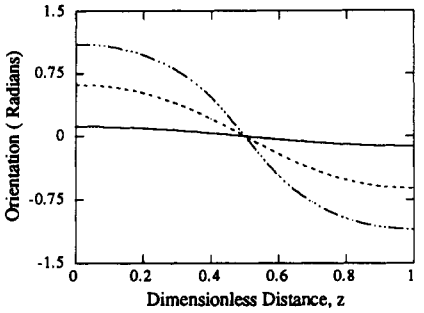

Figure 6. Evolution of the director orientation at the centerplane, $\theta(0.5,z)$, for $A = 1.4$ and $B = 1$. $H = 7.12 \times 10^3$ G; (—) time = 47.8 s; (- - -) time = 84 s; (-·····) time = 132 s.

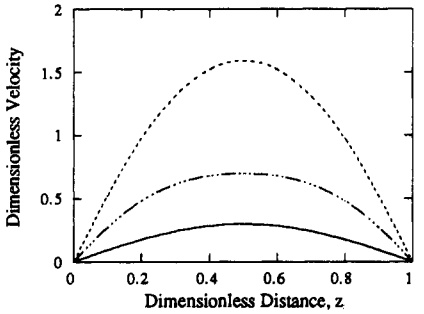

Figure 7. Evolution of the dimensionless velocity at the centerplane, $u(0.5,z)$, for $A = 1.4$ and $B = 1$. $H = 7.12 \times 10^3$ G; (—) time = 47.8 s; (- - -) time = 84 s; (-·····) time = 132 s.

= 0. The corresponding dimensionless velocity $u(y=0.5,z)$ profiles are shown in Figure 7. The counterrotating domains set up the transient flow; its intensity quickly decays as the magnetic free energy decreases to that of the elastic free energy.

This section shows that for the high-field regime the observed wavelength is independent of surface effects, and that it will be longer than that predicted by the linear theory, in agreement with the experimental findings,[4] and consistent with previous nonlinear analysis.[8] Furthermore, the magnitudes and dynamics of the director and velocity amplitudes are independent of surface effects. Finally, even for an orientational free surface, the director surface dynamics are much slower than that of the bulk.

3.2. Low-Field Long-Wavelength Regime. The director orientation $\theta(0.5,0)$ as a function of time is shown in Figure 8, for $A = 20$ (linear theory) and $A = 30$ and for the three representative surfaces. The corresponding maximum dimensionless velocity $u(0.5,0.5)$ as a function of time is shown in Figure 9. The figures show that at low fields there is a strong effect of the surface condition on the magnitudes and dynamics of the director and velocity amplitudes. The wavelength of the linear mode ($A = 20$) is the observed wavelength since for all surface conditions the amplitude of the director is the largest at all times, although the differences between the $A = 20$ and $A = 30$ modes are very small. The sensitivity to the surface condition follows from the scaled equations (1) and (2); at low fields ($A \to \infty$), there is a relative weak transmission of torques in the z direction when compared with the transmission in the y direction. The figures show that the linear mode (full line) is fastest at all times for all surface conditions. The adoption of longer wavelengths to quicken the decrease of the total free energy is not efficient in this regime because of the insensitivity to gradient changes in the z direction. The surface condition has a strong effect on the evolution and final value of the director amplitude since by decreasing B we are weakening the predominant restoring torques in the y direction. Since by decreasing B the director aligns faster and closer in the direction of

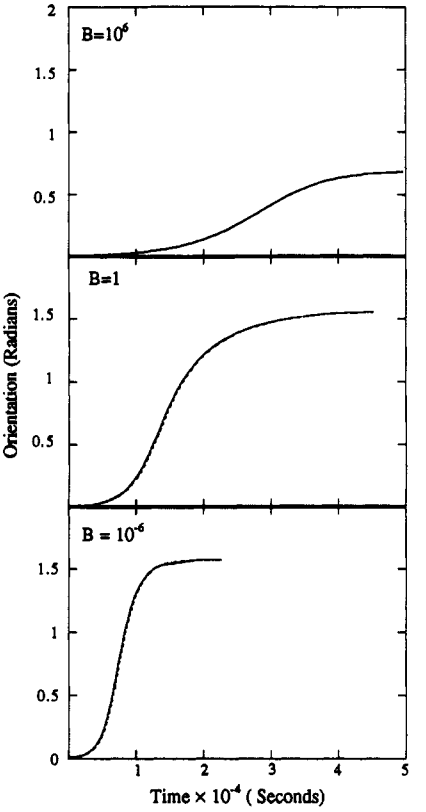

Figure 8. Orientation $\theta(0.5,0)$ of the director as a function of time, for $B = 10^6$, 1, and 10^{-6}. $H = 2.31 \times 10^3$ G; (—) $A = 20$ (linear); (- - -) $A = 30$.

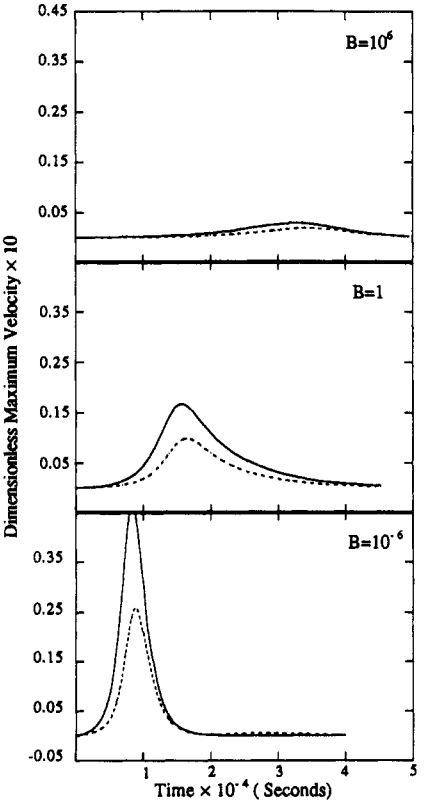

Figure 9. Maximum dimensionless velocity $u(0.5,0.5)$ as a function of time, for $B = 10^6$, 1, and 10^{-6}. $H = 2.31 \times 10^3$ G; (—) $A = 20$ (linear); (- - -) $A = 30$.

the applied field, the amplitude of the reorientation driven flows will achieve larger magnitudes at faster rates.

The total free energy per unit length in the x direction of the linear mode ($A = 20$) and for the normalized nonlinear mode ($A = 30$) is plotted in Figure 10 as a function

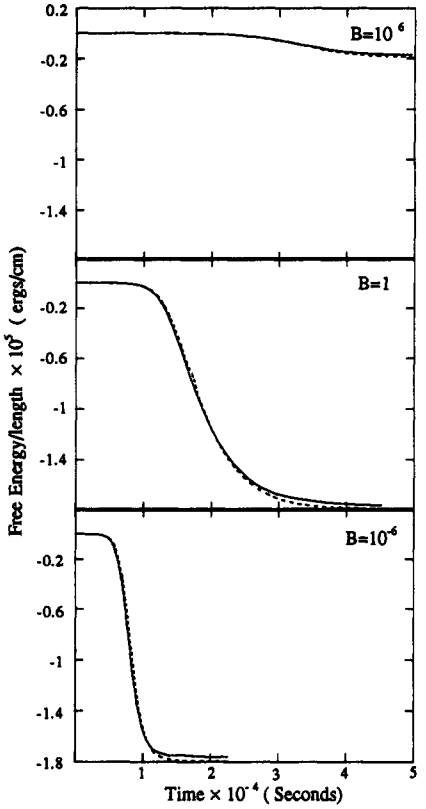

Figure 10. Free energy per unit length in the x direction as a function of time for $B = 10^6$, 1, and 10^{-6}. $H = 2.31 \times 10^3$ G; (—) $A = 20$ (linear); (- - -) $A = 30$. The free energy per unit length in the x direction is normalized with respect to the linear mode ($A = 20$): $F_{30}^* = 20F_{30}/30$.

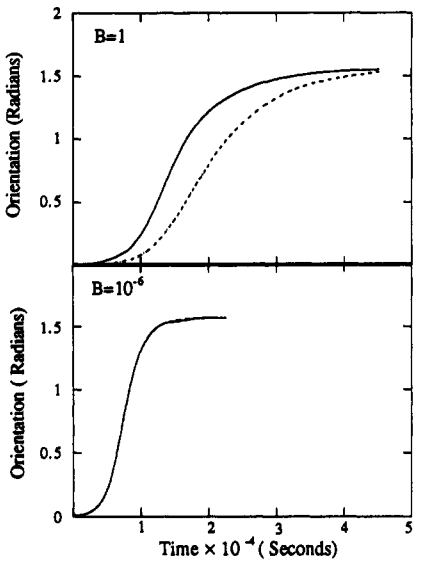

Figure 11. Comparison between representative bulk and surface director dynamics. Orientation of the director as a function of time for $B = 1$ and 10^{-6} and $A = 20$; $H = 2.31 \times 10^3$ G; (—) bulk director orientation $\theta(0.5,0)$; (- - -) surface director orientation $\theta(1,0)$.

of time, for the three representative surfaces. For each surface condition, the rate of decay of the free energy is almost equal for the two modes but is initially slightly faster for the linear mode. The small difference in total free energy between the two modes as the system approaches the steady state is due to a minor further alignment of the director in the direction of the field in a thin region centered at $z = 0.5$; this negligible driving force will certainly not produce the switch to a longer wavelength.

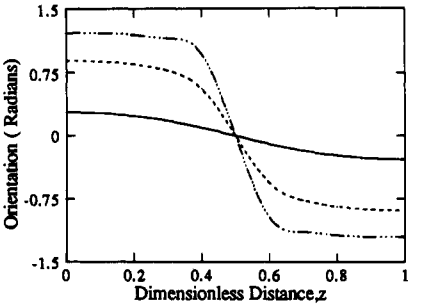

Figure 12. Evolution of the director orientation at the centerplane, $\theta(0.5,z)$, for $A = 20$ and $B = 1$. $H = 2.31 \times 10^3$ G; (—) time = 1.04×10^4 s; (- - -) time = 1.56×10^4 s; (-···-) time = 2×10^4 s.

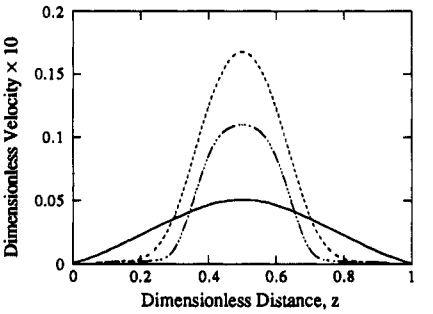

Figure 13. Evolution of the dimensionless velocity at the centerplane, $u(0.5,z)$, for $A = 20$ and $B = 1$. $H = 2.31 \times 10^3$ G; (—) time = 1.04×10^4 s; (- - -) time = 1.56×10^4 s; (-···-) time = 2×10^4 s.

The surface dynamics for the linear mode are summarized in Figure 11, where we plot the director orientation $\theta(0.5,0)$ and the director maximum surface orientation $\theta(1,0)$ as a function of time, for $B = 1$ and $B = 10^{-6}$. The reorientation surface and bulk time scales are now equivalent. This again reflects the fact that there is a strong transmission of torques in the y direction from the bulk into the surface due to the relative large values of A. The consequence of orientational slip is that the neighboring domains rotate around the normal to the surfaces without director gradients in the y direction.

The evolution of the director $\theta(y=0.5,z)$ profiles at the centerplane as a function of the dimensionless distance z is shown in Figure 12, for $A = 20$ and $B = 1$. The periodic distortions indicate clockwise director rotations for $z < 0.5$ and anticlockwise rotations for $z > 0.5$, but the profiles are now steplike (compare with Figure 6). The elastic torques transmitted in the z direction are negligible since only close to $z = 0.5$ is $\partial\theta/\partial z \neq 0$. The corresponding dimensionless velocity $u(y=0.5,z)$ profiles are shown in Figure 13. The counterrotating domains set up a flow only close to $z = 0.5$ where $\partial\theta/\partial z \neq 0$. This follows from the dominant terms in the infinity wavelength limit of eq 2:

$$\eta_1 \frac{\partial^2\theta}{\partial z \partial t} + \eta_6 A^2 \frac{\partial^2 u}{\partial y^2} = 0 \qquad (17)$$

where the first term represents the orientational force and the second term represents the viscous force due to the reorientation driven flow. Since $\partial\theta/\partial z \neq 0$ only in the proximity of $z = 0.5$, $u \neq 0$ only in that same region.

This section shows that the observed wavelength in the low-field regime will be the one predicted by the linear theory with no dependence on the surface effects, in agreement with the experimental results.[4] The magnitude and dynamics of the director and velocity amplitudes are strongly dependent on the surface conditions. Strong transmission of elastic torques in the y direction coupled

with orientational slip allows for the uniform reorientation in the vertical direction. Finally, reorientation driven flows and director gradients in the z direction are present only in the proximity of $z = 0.5$.

4. Conclusions

The Euler–Lagrange equation governing the transient surface director reorientation has been derived for the periodic twist instability of nematic polymers. For the studied cell spacing and nematic polymer properties, the dissipative interaction of the polymer and an isotropic surface has no effect on the observed wavelength of the periodic response. At low magnetic field strengths, the fastest decrease of the free energy of the periodic texture is that predicted by the linear theory; there is a strong surface effect on the amplitudes and on the time scale of the response. At high magnetic field strengths, the observed wavelength is longer than the one predicted by the linear theory; the amplitudes and time scales of the response are independent of surface effects. The predictions of the dependence of the observed wavelength on magnetic field strength are consistent with reported experimental results.[4]

Acknowledgment. This research is supported by a grant from the National Science and Engineering Research Council of Canada. I am grateful to the Computer Center of McGill University for the computer time provided.

Appendix

The coefficients $\{\eta_i\} = \{\eta_i'/\gamma_1\}$, $i = 1, ..., 6$, in eq 2 are given by

$$\eta_1' = \alpha_2 \cos^2\theta - \alpha_3 \sin^2\theta$$

$$\eta_2' = -(\alpha_2 - \alpha_3) \sin 2\theta$$

$$\eta_3' = \frac{1}{2}(\alpha_3 + \alpha_6) \sin 2\theta$$

$$\eta_4' = \frac{1}{2}\alpha_1 \sin 4\theta + \frac{1}{2}(\alpha_2 + \alpha_3) \sin 2\theta$$

$$\eta_5' = \frac{1}{4}\alpha_1(\sin 2\theta)^2 + \frac{1}{2}\alpha_4 + \frac{1}{2}(\alpha_5 - \alpha_2) \cos^2\theta + \frac{1}{2}(\alpha_3 + \alpha_6) \sin^2\theta$$

$$\eta_6' = \frac{1}{2}\alpha_4 + \frac{1}{2}(\alpha_3 + \alpha_6) \sin^2\theta$$

The contribution of the saddle splay to the free energy density is[23]

$$\Lambda_{sp} = (K_{22} + K_{24})\nabla\cdot[\mathbf{n}\nabla\cdot\mathbf{n} + \mathbf{n} \times \nabla \times \mathbf{n}] \quad (A.1)$$

Using the relations $n_x^2 + n_z^2 = 1$, $n_{x,y} = n_z\theta_y$, $n_{x,z} = n_z\theta_z$, $n_{z,y} = -n_x\theta_y$, $n_{z,z} = -n_x\theta_z$, $\theta = \theta(y,z)$, we obtain

$$[\mathbf{n}\nabla\cdot\mathbf{n} + \mathbf{n} \times \nabla \times \mathbf{n}] = -\frac{\partial\theta}{\partial z}\mathbf{i} \quad (A.2)$$

where $\mathbf{i}$ is the unit vector in the x direction. It follows that $\Lambda_{sp} = 0$ since $\partial(-\partial\theta/\partial z)/\partial x = 0$.

References and Notes

(1) Lonberg, F.; Fraden, S.; Hurd, A. J.; Meyer, R. B. *Phys. Rev. Lett.* **1984**, *52*, 1903.

(2) Fraden, S.; Hurd, A. J.; Meyer, R. B.; Cahoon, M.; Caspar, D. L. D. *J. Phys. Paris* **1985**, *46*, C3-85.

(3) Hurd, A. J.; Fraden, S.; Lonberg, F.; Meyer, R. B. *J. Phys. Paris* **1985**, *46*, 905.

(4) Fincher, C. R. *Macromolecules* **1986**, *19*, 2431.

(5) Srinivasarao, M. Ph.D. Thesis, Chemistry Department, Carnegie Mellon University, 1990.

(6) Srinivasarao, M.; Berry, G. C. *J. Stat. Phys.*, in press.

(7) Lonberg, F.; Meyer, R. B. *Phys. Rev. Lett.* **1985**, *55*, 718.

(8) Rey, A. D.; Denn, M. M. *Liq. Cryst.* **1989**, *4*, 409.

(9) Srajer, G.; Fraden, S.; Meyer, R. B. *Phys. Rev. A* **1989**, *39*, 4828.

(10) Goossens, W. J. A. *Mol. Cryst. Liq. Cryst.* **1985**, *124*, 305.

(11) de Gennes, P.-G. *The Physics of Liquid Crystals*; Oxford University Press: Oxford, 1975.

(12) Kleman, M.; Pikin, S. A. *J. Mec.* **1979**, *18*, 661.

(13) Hess, S.; Koo, H.-M., J. *Non-Equilib. Thermodyn.* **1989**, *14*, 159.

(14) Meyer, R. B. In *Polymer Liquid Crystals*; Ciferri, A., Krigbaum, W. R., Meyer, R. B., Eds.; Academic Press: New York, 1982.

(15) Morgan, P. W. *Macromolecules* **1977**, *10*, 1381.

(16) Panar, M.; Beste, L. F. *Macromolecules* **1977**, *10*, 1481.

(17) Taratuta, V. G.; Srajer, G. M.; Meyer, R. B. *Mol. Cryst. Liq. Cryst.* **1985**, *116*, 245.

(18) Vertogen, G. *Z. Naturforsch.* **1983**, *36A*, 1273.

(19) Ericksen, J. *Adv. Liq. Cryst.* **1979**, *2*, 233.

(20) Finlayson, B. A. *Nonlinear Analysis in Chemical Engineering*; McGraw-Hill: New York, 1980.

(21) Marrucci, G. *Mol. Cryst. Liq. Cryst.* **1982**, *72*, 153.

(22) Murthy, N. S.; Knox, J. R.; Samulski, E. T. *J. Chem. Phys.* **1976**, *65*, 4835.

(23) Dubois-Violette, E.; Parodi, O. *J. Phys. Colloq.* **1969**, *30*, C4-57.